

The precision measurement of the electron anti-neutrino spectrum in beta-decay of ^{144}Pr nuclei

A. V. Derbin,¹ I. S. Drachnev,¹ D. V. Ivanov,¹ I. M. Kotina,¹ V. N. Muratova,¹
N. V. Niyazova,¹ D. A. Semenov,¹ M. V. Trushin,¹ and E. V. Unzhakov¹

¹*St. Petersburg Nuclear Physics Institute NRC Kurchatov Institute, 188350 Gatchina, Russia*

(Dated: June 5, 2025)

The $^{144}\text{Ce} - ^{144}\text{Pr}$ electron antineutrino source is one of the most suitable radiochemical sources for experiments searching for the oscillations of active neutrinos to the light sterile state. In the current work the β -spectra of $^{144}\text{Ce} - ^{144}\text{Pr}$ source have been measured by two types of β -spectrometers based on silicon $\text{Si}(\text{Li})$ detectors in order to determine the energy spectrum of electron anti-neutrino emitted in the β -decay of ^{144}Pr nuclei. The nuclear form factor of the ground state beta transition in $^{144}\text{Pr} - ^{144}\text{Nd}$ has been obtained with high precision: $C(W) = 1 + (-0.0279 \pm 0.0003)W + (-0.076 \pm 0.003)W^{-1}$. The reduced cross section for the inverse beta decay reaction on hydrogen for the ^{144}Pr electron anti-neutrino source has been defined as $(4.7448 \pm 0.0006_{\text{stat}} \pm 0.012_{\text{syst}}) \times 10^{-44} \text{ cm}^2 \text{ decay}^{-1}$ that provides sufficient sensitivity to search for a sterile neutrino with a mass of $m_4 \sim 1 \text{ eV}$ and a mixing angle $\text{Sin}^2(2\theta_{14}) \sim 0.005$ using standard disappearance method.

I. INTRODUCTION

The three-flavor neutrino (ν_e, ν_μ, ν_τ) oscillations have been reliably observed using different neutrino sources and detectors. This fundamental discovery has demonstrated the presence of nonzero neutrino masses and has already went beyond the Standard Model (SM). Three mixing angles ($\theta_{12}, \theta_{23}, \theta_{13}$) and two mass difference squares $\Delta m_{12}^2, \Delta m_{23}^2$ of the Pontecorvo-Maki-Nakagawa-Sakata (PMNS) matrix have already been measured with acceptable accuracy [1]. However, the possible existence of additional sterile neutrino that mixes with the three SM neutrinos has remained one of the crucial unresolved problems of particle physics since the beginning of the century. The results of several neutrino experiments can be interpreted as indications of the light sterile neutrinos existence with Δm_{14}^2 of around 1 eV^2 [2].

The LSND experiment was the first one to observe $\approx 3\sigma$ excess of electron anti-neutrinos in the beam of neutrinos produced by pions decay at rest [3, 4]. The LSND results were tested by the MiniBooNE experiment which has also reported a low energy excess in $\nu_\mu \rightarrow \nu_e$ and $\bar{\nu}_\mu \rightarrow \bar{\nu}_e$ channels in neutrino beam from decay-in-flight pions. The overall significance of the MiniBooNE excess in both neutrino and antineutrino modes is 4.8σ [5–7]. The positive results of accelerator-based neutrino experiments LSND and MiniBooNE are currently being tested by JSNS² [8] and MicroBooNE [9, 10] collaborations.

The “reactor antineutrino anomaly” (RAA) has shown a $(5 - 6)\%$ discrepancy between the expected (based on a new anti-neutrino flux calculations [11, 12]) and the observed count rates of inverse beta-decay (IBD) reaction at the detectors installed close, $10 - 30 \text{ m}$, to the nuclear reactors. This effect has been explained via mixing between electron and sterile (anti)neutrino with oscillation parameters $\Delta m_{14}^2 \approx 1 \text{ eV}^2$ and $\text{sin}^2(2\theta_{14}) \approx 0.05$ [13, 14]. However, the recent results of reactor experiments [15–17], as well as the new data on the spectrum of reactor

neutrinos [18] probably do not confirm the existence of the RAA and its oscillation solution [19].

The next indication of the possible existence of a sterile neutrino has been related with $\approx 16\%$ (2.9σ) lack of count rate in Ga-Ge radiochemical solar neutrino detectors SAGE [20, 21] and GALLEX/GNO [22, 23] during calibration with intense artificial neutrino sources ^{51}Cr and ^{37}Ar . Recently, BEST collaboration has presented the new results obtained with ^{51}Cr source and Ga-Ge detector and the deficit of the observed $^{71}\text{Ga}(\nu_e, e^-)^{71}\text{Ge}$ reaction events stands at more than 5σ level [24, 25].

Several experiments with electron antineutrino sources (^{144}Ce , ^{106}Ru , ^{90}Sr and ^{42}Ar) were proposed to verify the detected anomalies by looking for neutrino oscillations at short distances [26, 27, 29]. One of these experiments was Borexino-SOX (Short distance neutrino Oscillations with BoreXino) in the Gran Sasso underground laboratory (Italy) with electron antineutrino ($\bar{\nu}_e$) $^{144}\text{Ce} - ^{144}\text{Pr}$ source [27, 28, 30–32]. The unprecedentedly low radioactive background of the Borexino detector, good energy and spacial resolutions together with large size allowing to perform an oscillometry (wave) measurement within the detector volume, and the well demonstrated capability to detect low energy electron antineutrinos have represented an ideal case for the study of short distance neutrino oscillations with artificial sources. Unfortunately, it was decided to suspend the Borexino-SOX experiment, however, the source $^{144}\text{Ce} - ^{144}\text{Pr}$ remains one of the most promising for the future experiments searching for light sterile neutrinos.

The expected sensitivity of the experiment with $^{144}\text{Ce} - ^{144}\text{Pr}$ source relative to the sterile neutrino oscillation parameters depends on the accuracy of flux determination as well as the energy spectrum shape for the electron anti-neutrino emitted in the β -decay of ^{144}Pr nuclei. The purpose of this work was a precise measurement of the β -spectra from $^{144}\text{Ce} - ^{144}\text{Pr}$ source and determination of the spectrum of electron anti-neutrinos

emitted in the decay ^{144}Pr nuclei with great precision.

II. EXPERIMENTAL SETUP

The spectra of the $^{144}\text{Ce} - ^{144}\text{Pr}$ source were measured by two setups: one using a beta-spectrometer in the classical "target - detector" configuration, and the other relies on an originally developed total absorption 4π -spectrometer consisting of a pair of Si(Li)-detectors. These measurements correspond to the application of two approaches to determining the detector response function - accurate M-C modeling and the use of a detector response function close to a Gaussian function.

A. Spectrometer "target-detector" type

The "target-detector" type spectrometer was created on the basis of a semiconductor Si(Li) detector with a thickness of 10.2 mm and the sensitive area diameter of 20 mm, which had the "top-hat" geometry (Fig. 1(A)). These dimensions ensure an effective absorption of electrons with energies up to 3 MeV.

The Si(Li)-detector produced from p-type single-crystal silicon with a resistivity of 4 k Ω cm and a carrier lifetime of 800 μs using standard technology that has been developed and tested by the Petersburg Nuclear Physics Institute. The characteristics of such detectors were described in [33–35].

The Si(Li)-detector was placed in a holder and equipped with a tungsten collimator with diameter of 12 mm. The total insensitive layer of the input detector window including the gold-plated *p*-contact was about 470 nm of silicon equivalent. The thickness of the insensitive layer of diffuse lithium on the back side of the detector was identified through the ratio of the total absorption peak areas for ^{241}Am source gamma lines with energies of 26.2 keV and 59.6 keV to be 420 μm .

The ^{144}Ce source in the form of a dried drop of colloidal solution was placed on the surface of a maylar substrate with thickness of 50 μm . The substrate was fixed in a delrin ring and placed on a supporting structure at the distance of 8.9 mm from the detector surface. The thickness distribution over the spot of the dried source ^{144}Ce was determined from the measured energy spectrum of alpha particles originating from the decays of ^{241}Am and ^{244}Cm , which were preserved in the source as low activity impurities after purification of the ^{144}Ce source. The average thickness of the source was determined as $\approx 1.0 \mu\text{m}$.

The entire installation of the Si(Li)-detector and ^{144}Ce source was placed in a vacuum cryostat and was cooled down to the temperature of liquid nitrogen (LN). The Si(Li)-detector was equipped with a charge-sensitive preamplifier with a field-effect transistor placed inside the vacuum cryostat and cooled down to the LN temperature. The negative bias voltage of 1 kV was applied directly to the gold coating of the detector.

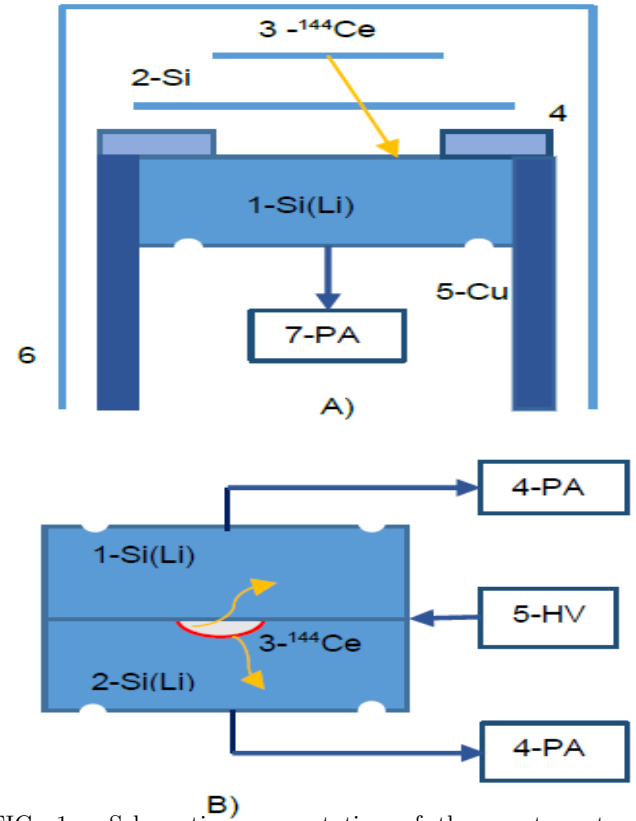


FIG. 1. Schematic representation of the spectrometers. A) "target - detector" spectrometer: 1 - Si(Li) full absorption detector, 2 - Si transition detector, 3 - $^{144}\text{Ce} - ^{144}\text{Pr}$ source, 4 - tungsten collimator, 5 - Cu cold finger, 6 - vacuum cryostat. B) 4π -spectrometer: 1,2 - Si(Li) full absorption detectors, 3 - $^{144}\text{Ce} - ^{144}\text{Pr}$ source, 4 - preamplifiers, 5 - bias voltage.

The signal from the preamplifier was registered by 8-channel CAEN v1725 digitizer with sampling rate of 250 MHz. Further transformations with the signal were performed digitally. The time reference and the record trigger of the event were formed on the basis of the signal after digital CR-2RC formation, while the amplitude analysis was performed using triangular shaping. The signals were recorded on event-by-event basis, a time reference and amplitude were recorded for each event.

The setup also included a scintillation detector based on a 3" (2.5 kg) bismuth orthogermanate (BGO) crystal coupled to a Hamamatsu R1307 PMT, the output of which was connected to the digitizer channel. Time and amplitude information was recorded for the signal of the BGO detector, which made it possible to analyze time-amplitude coincidences allowing to discriminate the β -spectrum of the allowed transition $^{144}\text{Pr} (0^-) \rightarrow ^{144}\text{Nd} (1^-)$. The time resolution of the spectrometric paths was about ~ 100 ns.

The energy calibration was performed with help of total absorption peaks for gamma quanta with energies of 570 keV and 1063 keV of the ^{207}Bi source (Fig. 2). The energy resolution FWHM (full width at half maximum), determined by the conversion electron peak with an en-

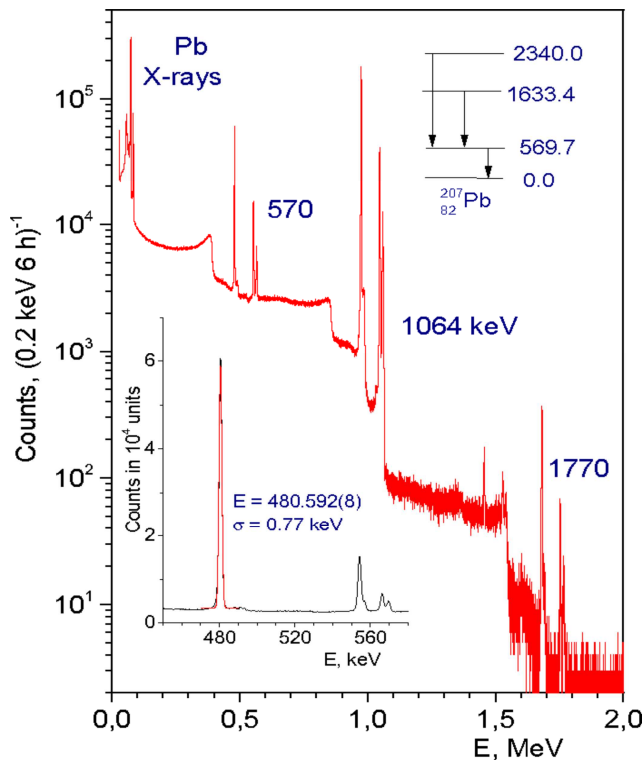


FIG. 2. Energy spectra in the ranges (0.01 – 2.0) MeV measured by a Si(Li)-detector with a ^{207}Bi source. The bottom insert shows the electron peaks corresponding to the internal conversion from K-, L- and M-shells while the 569.7 keV nuclear level discharge. The nuclear levels of ^{207}Pb are shown in the top inset.

ergy of 480.6 keV, was 1.8 keV ($\sigma = 770$ eV).

Measurements were carried out continuously for 2024 hours, with short technological stops. The long duration of the measurements was defined by the low activity of the ^{144}Ce source, which was ~ 15 Bk. The drift of the gain coefficient of the Si(Li) detector spectrometric channel during the long-term measurements was compensated by re-calibrations driven by the peak of conversion electrons with an energy of 91.5 keV at decays of ^{144}Ce and the 5.902 MeV α -peak of ^{244}Cm , which were presented in the measured spectra.

The “target - detector” type spectrometer has a number of undoubted advantages, in particular, it allows one to measure β -spectra of various sources using the same detector with quick replacement of the sources [35]. The main problem with the scheme is the backscattering of electrons from the crystal surface, which depends on the angle of incidence and leads to a large low-energy “tail” in the detector response function.

B. 4π -spectrometer

The original spectrometer with 4π geometry was designed on the basis of two Si(Li) detectors with the thicknesses of about 9 mm each, which exceeds the ionisation path of electrons with an energy of 3 MeV. The detectors were specially manufactured for this experiment and they were made in the “top-hat” shape with external diameters of 27 mm and 23 mm, height of 10 mm and diameters of the sensitive area of 20 mm and 18 mm. The Si(Li) detectors had different external diameters for the convenience of assembling the spectrometer with two detectors docked closely (Fig. 1, (B)) [36–38].

The characteristics of the detectors were tested in a separate vacuum cryostat using γ -, X-rays, conversion and Auger electrons from the $^{207}\text{Bi} \rightarrow ^{207}\text{Pb}$ source. The energy resolution measured for conversion electrons with energy of 481 keV from ^{207}Bi source was FWHM ≈ 2.0 keV for both detectors.

The total thickness of the insensitive layer of the Si(Li) detector, contributed by the deposited layers of palladium and gold and the surface layer of silicon, corresponds to a thickness of about 500 nm in silicon equivalent. Passing through such a thickness, electrons with energies of 20 keV and 3 MeV lose about 1 keV and 0.1 keV respectively.

Comparison of the measured intensities of X-ray $K_{\alpha 1}$, $K_{\alpha 2}$ and $K_{\beta 123}$ lead peaks with the results of Monte Carlo calculations using GEANT4.10.6 package allowed us to determine the thickness of the detector sensitive i-region. The useful thickness of both detectors determined in this way exceeds 8.5 mm, which ensures, if one does not takes into account the backscattering, the complete absorption of any electrons with the energies less than 3.3 MeV.

In the center of the front surface of one of the detectors a small cavity with a diameter of 5 mm and a depth of 1 mm was made by chemical etching. The ^{144}Ce β -source was placed into the cavity, directly onto the gold coating of the planar Si(Li) detector. The second detector was located on the detector with a cavity without any gap, and the bias voltage was applied to the resulting joined metal contact.

The assembly was placed in a vacuum cryostat and cooled down to the temperature of liquid nitrogen. The spectrometric channels were completely similar to the ones used in the “target-detector” type spectrometer and included preamplifiers with cooled field-effect transistors, the outputs of the preamplifiers were connected to the CAEN v1725 digitizer.

The total registered energy spectrum is obtained as the sum of the single event spectra from each of the Si(Li)-detectors and the total energy spectrum of events, recorded by both detectors in coincidence. The obtained spectrum solves the response function problem associated with backscattering of electrons from the detector surface.

The BGO-detector placed on the cryostat cap at a distance of 25 mm from the $^{144}\text{Ce} - ^{144}\text{Pr}$ source was also

connected to one of the inputs of the digitizer.

The proposed full absorption original 4π -spectrometer can be used for direct measurements of β -spectra and does not require corrections of the response function for the electrons backscattering from the crystal surface.

III. DATA ANALYSIS

The ^{144}Ce nucleus undergoes three first-order forbidden non-unique beta-decays to the ground ($Q_\beta = 318.7(8)$ keV, 76.5%) and excited levels 1^- ($Q_\beta = 238.6$ keV, 3.9% and $Q_\beta = 185.2$ keV, 19.6%) of the ^{144}Pr nucleus.

Decays of the ^{144}Pr to the ground ($Q_\beta = 2997.5(24)$ keV, 97.9%) and first excited ($Q_\beta = 2301.0$ keV, 1.04%) states of the ^{144}Nd nucleus correspond to first-order forbidden non-unique and unique transitions, respectively. Decay into the 1^- level of ^{144}Nd with an energy of 2185 keV ($Q_\beta = 811.8$ keV, 1.05%) is an allowed transition, the fitting of the beta spectrum does not require additional shape corrections as in the case of forbidden transitions [39].

The main objective of the work is to determine the spectrum of electron antineutrinos in the decay of ^{144}Pr with an energy above 1806 keV, the threshold of the inverse beta decay reaction on hydrogen. This is possible at electron energies less than 1192 keV in the case of a transition to the ground state and at an electron energy less than 495 keV in the decay to the first excited state.

The energy spectra of particles arising from the β -decay of ^{144}Ce , which are β -, Auger-, and conversion electrons, X- and γ -rays, have a complex form for fitting. Therefore, we will precisely fit the β -spectrum of ^{144}Pr in the range of (250 – 3100) keV, capturing a small region of the spectrum of ^{144}Ce near the end-point energy $Q_\beta(^{144}\text{Ce})$, in order to use it as an additional reference energy point. To determine the neutrino spectrum at neutrino energies greater than ($Q_\beta(^{144}\text{Pr}) - 250$ keV), extrapolation of the obtained β -spectrum to the low-energy region will be used.

In our work the detailed expression for electron energy spectrum of the given β -transitions included the following components [12, 40–43]:

$$S(W)dW = K pW (W - W_0)^2 F(Z, W) \cdot L_0(Z, W) S(Z, W) G_\beta(Z, W) C(Z, W) dW \quad (1)$$

where K is a normalization constant, p is electron momentum, W is total electron energy in units of electron mass ($W = T/mc^2 + 1$, T – kinetic energy of electron), W_0 corresponds to the endpoint energy of β -spectrum, Z is electric charge (i.e. proton number) of the daughter nucleus, and $F(Z, W)$ is Fermi function.

The first part $pW(W - W_0)^2$ of expression (1) is phase space factor accounting for distribution of decay energy between produced particles (i.e. electron and antineutrino). The second factor $F(Z, W)$ is so called Fermi

function describing the Coulomb interaction of outgoing electron with daughter nucleus. Fermi function originates from solution of Dirac equation in assumption of point-like and infinitely heavy nucleus and in fact represents the leading order QED correction for description of β -decay.

In case of high precision measurements the basic Fermi approximation becomes insufficient and one has to take more intricate effects into account, which is achieved by introducing additional electromagnetic and weak corrections accounting for finite size and mass of the daughter nucleus ($L_0(Z, W)$) [40], screening of nuclear electric field by electrons of atomic shell ($S(Z, W)$) [12, 42], and radiative correction due to emission of photons by charged particles involved in β -decay ($G_\beta(Z, W)$) [43, 46].

The screening correction $S(Z, W)$ accounts for the contribution of atomic electrons still remaining in “parent” configuration affecting the Coulomb potential of the “daughter” nucleus produced in β -decay. The initial work around for this problem suggested simple rescaling of the total energy of a β -particle $W = W - V_0$ [44], where V_0 is an effective shift of Coulomb potential due to the screening of atomic electrons. While this approach has been proven to be adequate for energies $\gg V_0$ [45], due to the energy rescaling this technique becomes invalid in low-energy part of the spectrum when $W \leq V_0$, exactly where it is of the most importance for evaluation of the high-energy end of corresponding neutrino spectrum.

In case of Ce and Pr atoms the screening shift $V_0 \approx 0.01$ MeV [42]. Since realistic description of screening correction below V_0 introduces significant complexity, we performed the upper estimate of potential uncertainty caused by screening effect by performing calculations for two border cases: no screening below V_0 ($F_{scr}(W) = 1$) and maximum screening below V_0 ($F_{scr}(W) = F_{scr}(V_0)$). These two options introduce the greatest uncertainty into the neutrino spectra and, as a consequence, into the expected count rate of the inverse beta decay events and were considered as the largest systematic uncertainty.

The radiative correction to the β -spectrum at order α has been computed in [46–48]. The radiative corrections have two components connected with the virtual photons on the Feynman lines of the charged particles and the emission of real internal bremsstrahlung (IB) photons [49]. As a result, when reconstructing the antineutrino spectrum from the β -spectrum, the correction $G_\beta(Z, W)$ is replaced not by $G_\beta(Z, W_0 - W)$, but a new correction $G_\nu(Z, W_\nu)$ [48, 49]. The β -spectrum and the antineutrino spectrum are described by two different radiative corrections $G_\beta(Z, W_e)$ and $G_\nu(Z, W_\nu)$, respectively. This approach should be used when determining the antineutrino spectrum based on “target-detector” spectrometer data since only 8.5% of the IB photons are emitted in the Si(Li)-detector solid angle.

The peculiarity of the described above 4π -spectrometer is that it registers with high efficiency the IB photons with energy up to 100 keV, which are considered as part of the radiative corrections. For example, 1 MeV electron appearing in ^{144}Pr -decay emits 75% of the IB pho-

tons with an energy of less than 100 keV, of which only 6% leave the 4π -detector without interaction. As a result, we used two different forms of the radiative correction function fitting the data of "target-detector" and 4π -spectrometer. For the 4π -spectrometer we used the correction $G_\nu(Z, W_\nu)$ introduced for the neutrino spectrum [48, 49] with the natural replacement of W_ν by $(W_0 - W_\nu)$.

In addition to electromagnetic and kinematic effects, another higher order correction to Fermi function arise from internal nuclear structure and matrix elements of a given β -transition. Nuclear shape-factor $C(Z, W)$ effectively accounts for complex collective nuclear interactions and becomes significant in case of forbidden transitions [43]. It is assumed that for allowed transitions $C(Z, W) = 1$, but except for some trivial cases of allowed and unique-forbidden transitions, analytical evaluation of nuclear shape-factor appears to be very difficult, thus leaving the experimental extraction the only viable option.

As noted above, we need to extrapolate the shape-factor $C(Z, W)$ to the region of electron energies below 250 keV. The encouraging fact is that the expected theoretical dependence of $C(Z, W)$ for the first-order forbidden non-unique $^{144}\text{Pr}(0^-) \rightarrow ^{144}\text{Nd}(0^+)$ transition $C(Z, W) \sim (p_e^2 + E_\nu^2 + 2\beta^2 E_\nu E_e)$ is almost constant in this region, smoothly increasing by only 7%.

The weak magnetism correction is not included in equation (1) because it is vanished for the main decay branch of ^{144}Pr -nucleus [50].

A. Analysis of the data of spectrometer "target-detector" type

The measured spectrum is a convolution of the beta spectrum (1) and the function $R(E, W)$ that describes the detector response to an electron with total energy W , while E is the energy recorded by the β -spectrometer. The response of the detector $R(E, W)$ was modeled by the Monte Carlo method using the GEANT4.10.6 package and G4Em_Standard.Physics_option4 package for the electromagnetic interactions, specially designed for detailed accounting of these interactions at low energies.

The simulation was carried out with a detailed description of the geometry of the installation and additional adjustment of the total thicknesses of the insensitive layers of the detector as well as the distribution of the thickness of the target, reproduced in the shape of the α -spectra of ^{244}Cm and ^{241}Am whose small impurities were present in the ^{144}Ce source. As an additional degree of freedom for back-scattered electrons, a variable ratio was introduced for the areas of the response function for electron energy E below and above the original electron energy reduced by 25 keV ($T - 25$ keV).

The analysis of the "target - detector" experimental data was rather sophisticated as the duration of ^{144}Ce source storage time by the moment of the experiment begin was already 410 days, resulting thus in low activity

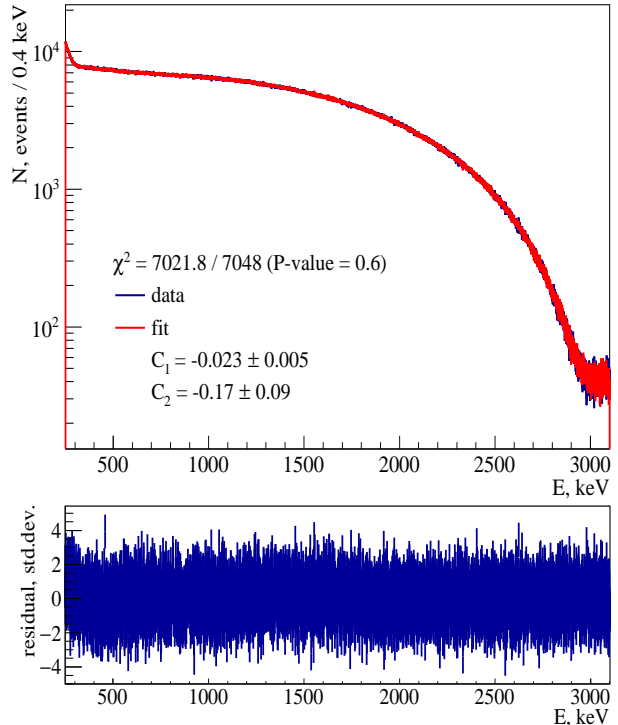


FIG. 3. The measured spectrum of the ^{144}Ce - ^{144}Pr source with the spectrometer in the "target-detector" geometry. The fitting result is shown by red line. The difference is given in the units of standard deviations (SD).

and a complex composition of the background components in the measured spectrum. In order to solve this problem, the results of the long-term measurements were divided into two consecutive datasets. The analysis of the difference between the first and second parts of the dataset made it possible to significantly reduce the contribution of long-lived background components at the cost of losing statistics from the decays of ^{144}Ce and ^{144}Pr . As a result of the measurements, 2024 one-hour series were selected, which were divided into two equal parts. The spectrum corresponding to the first part was fitted by the sum of the second part spectrum, the beta spectra of ^{144}Ce and ^{144}Pr and the complementary background components (Fig. 3).

The main background component present in the measured spectrum was associated with the activity of the ^{154}Eu ($\tau = 12.4$ y). The expected spectrum of ^{154}Eu was simulated by the Monte Carlo method similarly to the response function. The spectrum measured over 1012 hours was fitted with the maximum likelihood method using the χ^2 function (Fig. 3). The fitting was carried out in the range (250 – 3100) keV, which includes part of the β -spectrum of ^{144}Ce . This made it possible to use the well-established Q_β -value (318.7(8) keV) of ^{144}Ce -decay.

The nuclear shape-factor $C(Z, W)$ is the function

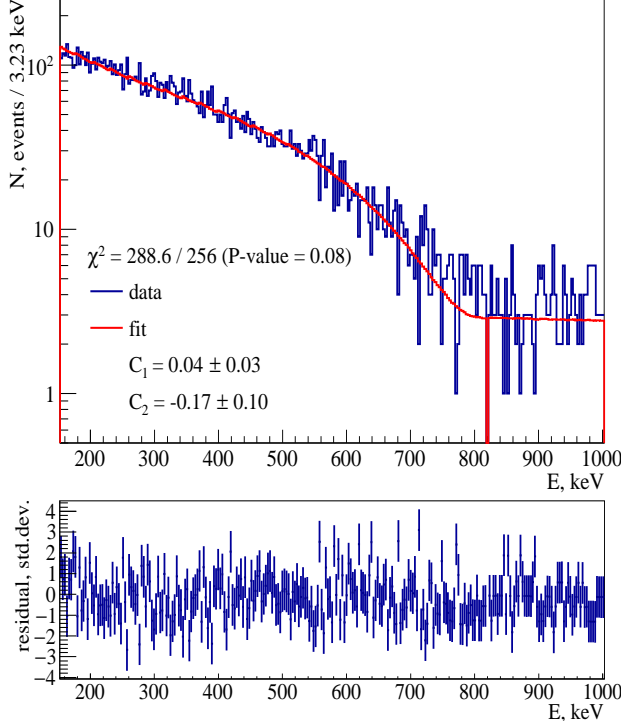


FIG. 4. The spectrum of the allowed β -transition $^{144}\text{Pr} (0^-) \rightarrow ^{144}\text{Nd} (1^-)$ measured with the “target-detector” spectrometer and the fitting results.

searched in the problem of the β -spectrum measurement. The form factor was parameterized in powers of W similarly to [51]:

$$C(W) = 1 + C_1 W + C_2 W^{-1}, \quad (2)$$

where C_1 and C_2 are free parameters. As a result of the analysis, the following expression for the form factor function was obtained:

$$C(W) = 1 + (-0.023 \pm 0.005)W + (-0.17 \pm 0.09)W^{-1}. \quad (3)$$

The accuracy of the obtained result (3) is limited by the weak activity of the ^{144}Ce source, which requires a small distance from the detector to the target, that leads to large angles of incidence of electrons onto the crystal surface and an increased proportion of backscattered electrons. The accuracy in determination of the the nuclear form factor parameters C_1 and C_2 could be significantly increased by usage of a more active source with “target-detector” spectrometer.

The spectrum of the allowed transition $^{144}\text{Pr} (0^-) \rightarrow ^{144}\text{Nd} (1^-)$, fitted similarly with the background component of random coincidences, has shown a good agreement of the model with the experiment (Fig. 4). The fit with fixed $C_1 = 0$ and $C_2 = 0$ gives the minimum χ^2 -value is 288.6 for 256 degrees of

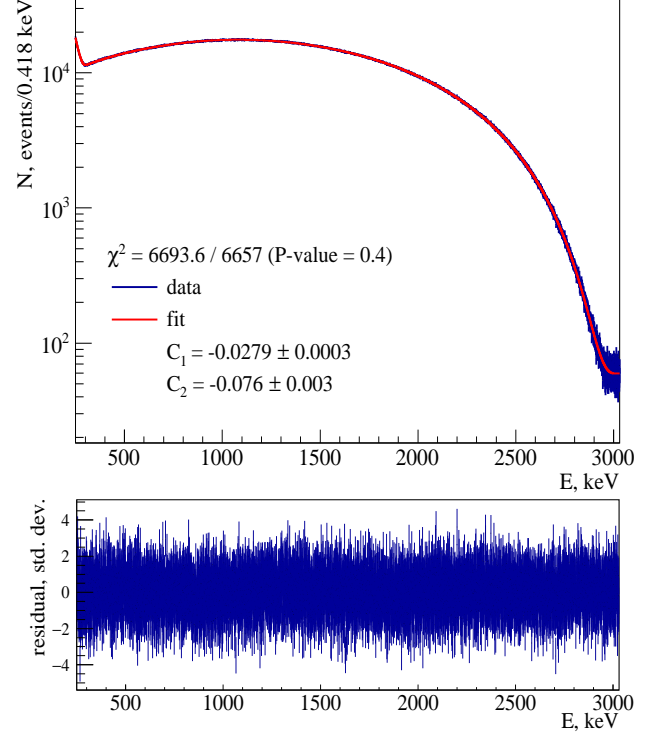


FIG. 5. The energy spectrum of the ^{144}Ce - ^{144}Pr source measured with the 4π -spectrometer (blue points) and the fitting results (red line). The difference is shown in the units of standard deviations (SD).

freedom, which corresponds to the acceptable P -value = 0.08. If the parameters C_1 and C_2 are free during the fit, their best-fit values are compatible with zero within their uncertainties.

B. Analysis of the data of 4π -spectrometer

Neglecting the energy of the recoil nucleus, the energy of the electron and neutrino are related by a simple relation $E_e + E_\nu = Q_\beta$. The 4π detector geometry makes it possible to measure the real spectrum of electrons and, ideally in the case of delta response $R(E, W)$, allows one to directly determine the antineutrino spectrum from the measured electron one without using the fitting procedure based on eq.(1). However, at electron energies where transitions to excited states of ^{144}Pr or decays of ^{144}Ce contribute to the measured spectrum, corrections must be made for the corresponding branching factors.

Although the response of the 4π spectrometer is close to the Gaussian function, one should take into account the passage of the insensitive layers of the source and detectors. In order to account for these effects detailed M-C calculations were carried out for different electron energies.

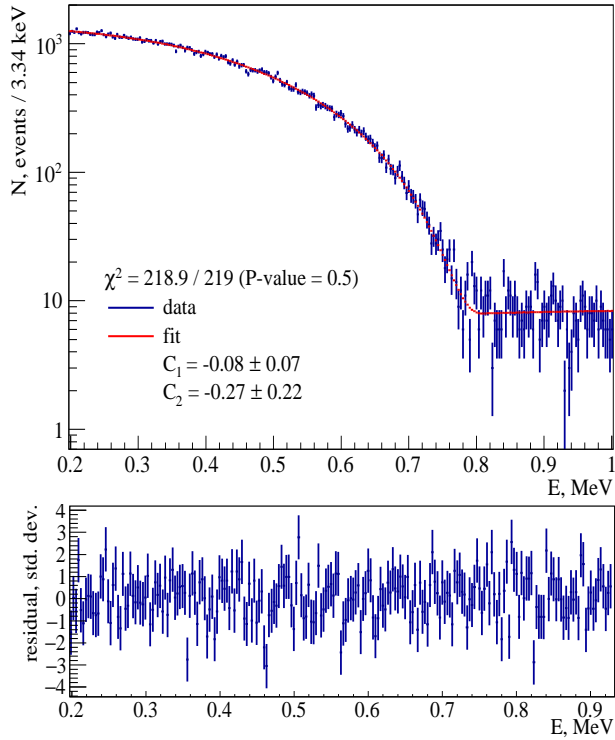


FIG. 6. The energy spectrum of the allowed β -transition $^{144}\text{Pr} (0^-) \rightarrow ^{144}\text{Nd} (1^-)$ measured with the 4π -spectrometer and the fitting results.

The detector response function $R(E, W)$ determined as a result of fitting looks like as a convolution of a Gaussian function with an exponential tail, which describes small energy losses in the target and non-sensitive layers of the detectors. As an example, for 1 MeV electrons the standard deviation for response function (the square root of the second central moment σ^2) is 56.8 keV and the fraction of electrons detected with an energy less then 0.850 MeV is 3.4%.

The response function calculated by the M-C method was described analytically as:

$$R(E, W) = \exp(P_0(W) + E/P_1(W))\theta(T - E). \quad (4)$$

The function $P_0(W)$ was estimated from the condition of conservation of the full integral of the response function. $P_1(W)$ describes the dependence of the standard deviation of the response function $\sigma_{RF}(W)$ with two additional free parameters p_1 and p_2 : $\sigma_{RF}(W) = \sigma_{MC}(W)(1 + p_1W + p_2W^2)$, where the dependence $\sigma_{MC}(W)$ is obtained by the Monte Carlo method. The parameters p_1 , p_2 are responsible for imperfections in the modeling, $\theta(x)$ is the Heaviside step function.

The spectrum of $^{144}\text{C} - ^{144}\text{Pr}$ source measured by 4π β -spectrometer over 106 hours is shown in Fig. 5. The fitting was carried out by the maximum likelihood method with the χ^2 likelihood function with the shape factor

$C(Z, W)$ similar to the one (2) used in the data analysis of the “target-detector” spectrometer.

As a result of the analysis, the following values of the parameters C_1 and C_2 of the nuclear form factor function were obtained:

$$C(W) = 1 + (-0.0279 \pm 0.0003)W + (-0.076 \pm 0.004)W^{-1}. \quad (5)$$

From (3) and (5) one could see that the results for the parameters C_1 and C_2 obtained with two different beta spectrometers agree with each other within the uncertainties (Fig.3 and Fig.5). The achieved accuracy of C_1 and C_2 determination in the measurement with the 4π spectrometer is significantly higher than for the “target detector” setup. The fitting of the allowed transition measured spectrum has shown a good agreement of the theoretical model used with the experiment as in the case of the measurement with the target-detector spectrometer (Fig. 6).

The ^{144}Pr β -spectrum has been previously measured in several works [51–55] that used different expressions for the $F(Z, W)$ Fermi function and for the $C(Z, W)$ form factor. Therefore, a direct comparison of the results obtained is difficult. Nevertheless, our result for $C(Z, W)$ is more precise but consistent with [54, 55] within experimental uncertainties.

IV. NEUTRINO SPECTRUM

Since the β -spectrum shape measured by the 4π -spectrometer turns out to be more accurate, it was used to determine the neutrino spectrum. Provided there is a measured shape of each component of β -spectrum one could evaluate a neutrino spectrum though conservation of energy in the decay as the total energy of each decay is given by its endpoint energy. The neutrino spectrum $N(E_\nu)$ is obtained from (1) by the replacements W with $E_\nu = (W_0 - W)$.

The main interest of sterile neutrino experiments lies above the energy threshold of inverse beta decay on hydrogen, both in terms of shape and spectrum fraction. As for $^{144}\text{Ce} - ^{144}\text{Pr}$ source, only two β -transitions contribute to the neutrino spectrum above this threshold: $^{144}\text{Pr}(0^-) \rightarrow (0^+)^{144}\text{Nd}(0^+)$ and $^{144}\text{Pr}(0^-) \rightarrow ^{144}\text{Nd}(2^+)$ with the branching ratios of 97.9% and 1.04%, respectively.

Fig. 7 illustrates the spectrum $N(E_\nu)$ of electron antineutrinos from ^{144}Pr source. The numerical values $N(E_\nu)$ for neutrinos with energies above the IBD threshold are shown in the Tab. I. The uncertainties of $N(E_\nu)$ are calculated with toy Monte-Carlo method based on the uncertainties of the evaluated form-factor parameters C_1 and C_2 from (5) and taking into account their correlation. The parameters evaluated with this method were simulated 10000 times and used for performing 2-dimensional spectrum density plot. The RMS of density distributions of its monoenergetic projections was taken as the statistical uncertainty of the spectrum.

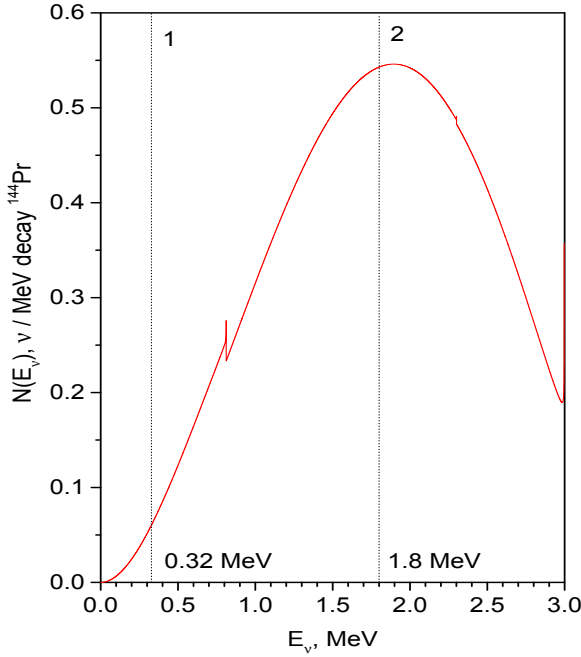


FIG. 7. The energy spectrum of electron antineutrinos of the ^{144}Pr source. Numerical values for $E_\nu \geq 1.8$ MeV are given in Tab. I.

The uncertainty of the energy scale E_ν is determined by the accuracy of the Q_β -value of β -transition of the ^{144}Pr to the ground state of ^{144}Nd [39].

Neutrinos from the decay of ^{144}Ce have the same intensity as ^{144}Pr -neutrinos, but their energies are less than 318 keV (the region to the left of line 1 in Fig. 7). The threshold value of the IBD reaction on hydrogen in the laboratory system is 1.806 MeV (line 2).

Considering the precision given by our measurement one could apply toy Monte-Carlo to convert the uncertainties on the form-factor parameters to the fraction of the ^{144}Pr β -spectrum above the threshold IBD reaction that is $(0.50192 \pm 0.00006_{\text{stat}} \pm 0.00065_{\text{syst}})$ so the statistic precision of this value is as low as 0.01 %. The systematic uncertainty evaluated as the difference of the values derived for two boundary cases of low-energy screening correction is 0.00022 (0.044 %). Greater systematic error is associated with the uncertainty of the energy scale at 1.806 MeV that lead to 0.0065 (0.13 %).

The expected number of IBD events is determined by the integral of the product of the reaction cross section $\sigma(E_\nu)$ and the neutrino flux $N(E_\nu)$ (Fig. 8). Using the cross section of IBD reaction [56–59], one could evaluate the experimental neutrino count rate, that is $\sigma_{144Pr} = (4.7448 \pm 0.0006_{\text{stat}} \pm 0.012_{\text{syst}}) \times 10^{-44}$ cm² per one decay of ^{144}Pr nucleus. The errors reported here

TABLE I. Neutrino spectrum data ($N(E_\nu)$) for energies above the threshold of IBD reaction. The error values (1σ) are shown in parentheses.

E, keV	N, 1/MeV	E, keV	N, 1/MeV	E, keV	N, 1/MeV
1809	0.54230(80)	2209	0.49961(79)	2609	0.35291(74)
1819	0.54259(80)	2219	0.49713(79)	2619	0.34837(73)
1829	0.54281(80)	2229	0.49459(79)	2629	0.34378(73)
1839	0.54297(80)	2239	0.49198(79)	2639	0.33916(73)
1849	0.54306(80)	2249	0.48931(79)	2649	0.33451(73)
1859	0.54308(80)	2259	0.48658(79)	2659	0.32983(72)
1869	0.54302(80)	2269	0.48378(78)	2669	0.32511(72)
1879	0.54290(80)	2279	0.48093(78)	2679	0.32037(72)
1889	0.54271(80)	2289	0.47803(78)	2689	0.31559(72)
1899	0.54245(80)	2299	0.47388(78)	2699	0.31079(71)
1909	0.54211(80)	2309	0.46789(78)	2709	0.30597(71)
1919	0.54171(80)	2319	0.46485(78)	2719	0.30112(71)
1929	0.54124(80)	2329	0.46174(78)	2729	0.29625(71)
1939	0.54070(80)	2339	0.45858(78)	2739	0.29137(70)
1949	0.54008(80)	2349	0.45535(78)	2749	0.28646(70)
1959	0.53940(80)	2359	0.45207(78)	2759	0.28154(70)
1969	0.53864(80)	2369	0.44873(77)	2769	0.27661(69)
1979	0.53782(80)	2379	0.44532(77)	2779	0.27166(69)
1989	0.53693(80)	2389	0.44187(77)	2789	0.26671(69)
1999	0.53596(80)	2399	0.43835(77)	2799	0.26174(68)
2009	0.53492(80)	2409	0.43479(77)	2809	0.25677(68)
2019	0.53382(80)	2419	0.43116(77)	2819	0.25180(68)
2029	0.53264(80)	2429	0.42749(77)	2829	0.24683(67)
2039	0.53139(80)	2439	0.42375(76)	2839	0.24186(67)
2049	0.53008(80)	2449	0.41997(76)	2849	0.23691(67)
2059	0.52869(80)	2459	0.41614(76)	2859	0.23196(66)
2069	0.52723(80)	2469	0.41225(76)	2869	0.22703(66)
2079	0.52571(80)	2479	0.40831(76)	2879	0.22212(65)
2089	0.52411(80)	2489	0.40432(76)	2889	0.21723(65)
2099	0.52244(80)	2499	0.40028(76)	2899	0.21238(65)
2109	0.52071(80)	2509	0.39620(75)	2909	0.20757(64)
2119	0.51891(79)	2519	0.39207(75)	2919	0.20280(64)
2129	0.51703(79)	2529	0.38789(75)	2929	0.19809(64)
2139	0.51509(79)	2539	0.38367(75)	2939	0.19345(63)
2149	0.51308(79)	2549	0.37940(75)	2949	0.18888(63)
2159	0.51100(79)	2559	0.37509(75)	2959	0.18442(62)
2169	0.50886(79)	2569	0.37073(74)	2969	0.18011(62)
2179	0.50665(79)	2579	0.36634(74)	2979	0.17610(62)
2189	0.50437(79)	2589	0.36190(74)	2989	0.17327(62)
2199	0.50202(79)	2599	0.35743(74)	2995	0.22220(80)

are due only to uncertainties in the neutrino spectrum of ^{144}Pr connected with the shape $N(E_\nu)$ (mainly due to the uncertainty in the screening correction 0.0041 (0.09%) and energy scale E_ν). The latter can be substantially improved by any refinement of the Q_β -value of ^{144}Pr -decay. The obtained precision of σ_{144Pr} in 0.25% would correspond to an experimental uncertainty of neutrino count rate expected for a sterile neutrino experiment using ^{144}Ce – ^{144}Pr source. In this case this value would be sub-dominated by other experimental uncertainties, e.g. the precision of the source calorimetry for Borexino-SOX experiment has reached precision of 0.4% [30].

We can also provide an analytical interpolation of the spectrum, that could be expressed in two energy intervals. For neutrino energies E above the unique forbidden transition endpoint of 2.301 MeV, the spectrum is interpolated as follows:

$$N(E)_{(2.3)\text{MeV}} = a_1 + a_2E + a_3E^2 + a_4E^3 + a_5E^4 + \exp(a_6 + a_7E^2) + \exp(a_8 + a_9E^3). \quad (6)$$

Between the inverse beta decay threshold of 1.806 MeV and 2.301 MeV, we also include a transition to the excited level of $0^- \rightarrow 2^+$ in ^{144}Nd , adding an additional component $N(E)_{(2.3)\text{MeV}}$:

$$N(E)_{(1.8)\text{MeV}} = N(E)_{(2.3)\text{MeV}} + a_{10} + a_{11}E + a_{12}E^2 + a_{13}E^3, \quad (7)$$

where the parameters are defined according to the Tab. II. The accuracy of this analytical interpolation could be estimated by the ratio of two integrals: the product of the measured spectrum with the cross section of the inverse beta decay and the product of the interpolation function with the same cross section. For neutrino energies greater than 1.8 MeV, the deviation of these two values was found to be as low as 0.4 %.

TABLE II. Parameters of neutrino spectrum analytical description above 1.8 MeV.

a_1	1.12×10^{-2}	a_8	$-8.19 \times 10^{+2}$
a_2	-1.79×10^{-5}	a_9	3.01×10^{-8}
a_3	1.14×10^{-8}	a_{10}	-6.29×10^{-3}
a_4	-3.21×10^{-12}	a_{11}	8.21×10^{-6}
a_5	3.30×10^{-16}	a_{12}	-3.57×10^{-9}
a_6	$-1.52 \times 10^{+2}$	a_{13}	5.19×10^{-13}
a_7	1.56×10^{-5}		

V. CONCLUSION

The β -spectra of the $^{144}\text{Ce} - ^{144}\text{Pr}$ source were studied using two spectrometers based on semiconductor Si(Li) detectors. The spectra were measured using a beta spectrometer in the classical “target-detector” scheme and with an original 4π full absorption spectrometer consisting of two of Si(Li) detectors. The models of the beta spectrometer response function calculated through the Monte Carlo simulation were tested by fitting the

spectrum of the allowed beta transition $^{144}\text{Pr} (0^-) \rightarrow ^{144}\text{Nd} (1^-)$ and have shown good agreement between the response models and experimental data. The function of the nuclear form factor of the ground state beta transition in $^{144}\text{Pr} - ^{144}\text{Nd}$ has been defined as $C(W) = 1 + (-0.0279 \pm 0.0003)W + (-0.076 \pm 0.004)W^{-1}$. The electron antineutrino spectrum of the ^{144}Pr decays was obtained from the measured β -spectrum and the $C(W)$

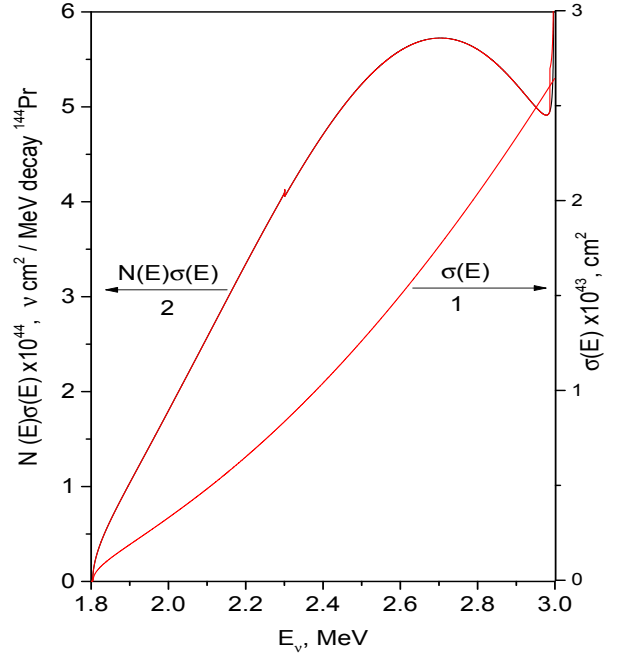


FIG. 8. The cross-section of inverse beta-decay ($\sigma(E_\nu)$) and a product of $\bar{\nu}$ -spectra of the ^{144}Pr ($N(E_\nu)$) and the cross-section.

form factor parameters. The reduced cross section for the inverse beta decay reaction for the ^{144}Pr electron anti-neutrino source is $(4.7448 \pm 0.0006_{\text{stat}} \pm 0.012_{\text{syst}}) \times 10^{-44} \text{ cm}^2$ per ^{144}Pr decay which is the most accurate measurement up to date.

ACKNOWLEDGEMENTS

This work has been supported by Russian Science Foundation (project no.24-12-00046).

-
- [1] S. Navas et al., (Particle Data Group), Phys. Rev. D 110, 030001 (2024)
 [2] M.A. Acero, C.A. Argüelles, M. Hostert et al., White Paper on Light Sterile Neutrino Searches and Related Phenomenology, arXiv:2203.07323v2 [hep-ex] 18 May 2023

- [3] C. Athanassopoulos et al. (LSND Coll.), Phys. Rev. Lett. 77 (1996) 3082.

- [4] A. Aguilar et al. (LSND Collaboration), Phys. Rev. D 64 (2001), 112007
- [5] A.A. Aguilar-Arevalo et al. (MiniBooNE Coll.), Phys. Rev. Lett. 102 (2009), 101802
- [6] A.A. Aguilar-Arevalo et al. (MiniBooNE Coll.), Phys. Rev. Lett. 120 (2018), 141802
- [7] A.A. Aguilar-Arevalo et al. (MiniBooNE Coll.), Phys. Rev. D 103 (2021), 052002
- [8] D.H. Leea, S.Ajimura, M.K. Cheoun et al. arXiv:2308.02722v1 [hep-ex] 4 Aug 2023
- [9] P. Abratenko et al. (MicroBooNE Coll.), Phys. Rev. Lett. 128 (2022), 111801
- [10] P. Abratenko et al. (MicroBooNE Collaboration), Phys.Rev. Lett. 128, 241801 (2022)
- [11] T.A. Mueller et al. Phys. Rev. C 83 (2011) 054615.
- [12] P. Huber Phys. Rev. C 84 (2011) 024617.
- [13] M. Dentler, A. Hernandez-Cabezudo, J. Kopp, M. Maltoni and T. Schwetz, JHEP 11 (2017).
- [14] S. Gariazzo, C. Giunti, M. Laveder and Y. F. Li, Phys. Lett. B 782 (2018), 13.
- [15] D. Adey et al. (Daya Bay Coll.), Phys. Rev. Lett. 123, 111801 (2019).
- [16] G. Bak et al. (RENO Coll.), Phys. Rev. Lett. 122, 232501 (2019).
- [17] H. Almazán, L. Bernard, A. Blanchet et al. (STEREO Coll.) Nature, 613, 7943, 257, (2023)
- [18] V. Kopeikin, M. Skorokhvatov and O. Titov, Phys. Rev. D 104 (2021) no.7, L071301
- [19] C. Giunti, Y.F. Li, C.A. Ternes, Z. Xin, arXiv:2110.06820v2 (2021)
- [20] J.N. Abdurashitov et al. (SAGE Coll.), Phys. Rev. C 59 (1999), 2246
- [21] J.N. Abdurashitov et al. (SAGE Coll.), Phys. Rev. C 73 (2006) 045805
- [22] W. Hampel et al. (GALLEX Coll.), Phys. Lett. B 420 (1998), 114
- [23] M. Altmann et al. (GNO Collab.), Phys. Lett. B 616 174 (2005)
- [24] V.V. Barinov et al. Phys. Rev. Lett. 128 (2022) no.23, 232501
- [25] V. Barinov and D. Gorbunov, Phys. Rev. D 105 (2022) no.5, L051703
- [26] M. Cribier et al. Phys. Rev. Lett. 107 (2011) 201801.
- [27] G. Bellini et al. (Borexino-SOX Coll.) JHEP08 (2013) 038
- [28] L. Di Noto, M. Agostini, K. Althenmuller, G. Bellini et al. (Borexino-SOX Coll.) IL Nuovo Cimento 38 C (2015) 36
- [29] A. Gando, Y. Gando, S. Hayashida et al. (CeLAND Coll.) arXiv:1312.0896v2 13 Apr 2014
- [30] K. Altenmüller, M. Agostini, S. Appel, G. Bellini et al. (Borexino-SOX Coll.) Physics of Atomic Nuclei, 79, 1481, (2016).
- [31] M. Pallavicini et al. (Borexino-SOX Coll.) J. Phys. Conf. Ser., 888, 012018, (2017).
- [32] M. Gromov et al. (Borexino-SOX Coll.) J. Phys. Conf. Ser., 934, 012003, (2017).
- [33] N.V. Bazlov, S.V. Bakhlanov, A.V. Derbin, I.S. Drachnev, V.K. Eremin, I.M. Kotina, V.M. Muratova, N.V. Pilipenko, D.A. Semenov, T.V. Unzhakov, E.A. Chmel', Instrum. Exp. Tech., 63, 323 (2018),
- [34] I.E. Alekseev et al. Nucl. Instr. and Meth. A890, 64, (2018).
- [35] I.E. Alekseev et al. Phys. Rev. C 102, 064329 (2020)
- [36] I.E. Alekseev et al. Instruments and Experimental Techniques, 64, 190, (2021).
- [37] I.E. Alekseev et al. J. of Phys.: Conf. Ser., 2103, 012144, (2021).
- [38] S.V. Bakhlanov S. V. et al. Physics of Atomic Nuclei, 85, 936 (2022)
- [39] <https://nds.iaea.org/>
- [40] D. Wilkinson, NIM-A, 290, 509 (1990)
- [41] H. Behrens and W. Bühring, Nucl. Phys. A 162, 111 (1971)
- [42] H. Behrens and W. Bühring, *Electron Radial Wave Functions and Nuclear Beta Decay*, Clarendon, Oxford, (1983)
- [43] L. Hayen, N. Severijns, K. Bodek, D. Rozpedzik, X. Mougeot, Rev. Mod. Phys., 1, 015008 (2018)
- [44] M.E. Rose, Phys. Rev., 49, 727 (1936)
- [45] J.J. Matese, W.R. Johnson, Phys. Rev. 150, 846 (1966)
- [46] A. Sirlin, Phys. Rev. 164, 1767 (1967).
- [47] A. Sirlin, Rev. Mod. Phys. 50, 573 (1978)
- [48] A. Sirlin, Phys. Rev. 84, 014021 (2011)
- [49] I. S. Batkin and M. K. Sundaresan, Phys. Rev. D 52, 5362 (1995)
- [50] A.C. Hayes, J.L. Friar, G.T. Garvey, G. Jungman, G. Jonkmans, Phys. Rev. Lett. 112 202501 (2014)
- [51] M.J. Laubitz, Proceedings of the Physical Society. Section A, 69, 789 (1956)
- [52] R.L. Graham, J.S. Geiger and T.A. Eastwood, Can. Journ. Phys., 36, 1084 (1958).
- [53] F.T. Porter, P.P. Day, Phys. Rev., 114, 1286 (1959)
- [54] H. Daniel, G.Th. Kaschl, Nuclear Physics, 76, 97 (1966)
- [55] T. Nagarajan, M. Ravindranath, K. Venkata Reddy, Il Nuovo Cimento A3, 699 (1971)
- [56] A. Strumia and F. Vissani, Phys.Lett. B564, 42 (2003)
- [57] G. Ricciardi, N. Vignaroli, F. Vissani, JHEP 08, 212 (2022)
- [58] G. Ricciardi, N. Vignaroli, F. Vissani, arXiv:2502.17343v1
- [59] We used the analytical expression for the IBD cross-section from [56], adjusted to fit the data [57] by two linear functions in (1.8-2.02) MeV and (2.02-3.0) MeV regions.